ELSEVIER

Journal of Photochemistry and Photobiology A: Chemistry 121 (1999) 17–25

Journal of Photochemistry and Photobiology A:Chemistry

Intramolecular charge transfer and photoisomerization of 2-(*p*-dimethylaminostyryl)benzoxazole: A new fluorescent probe

Tarek A. Fayed

Chemistry Department, Faculty of Science, Tanta University, 31527, Tanta, Egypt

Received 28 July 1998; received in revised form 12 November 1998; accepted 13 November 1998

Abstract

2-(*p*-Dimethylaminostyryl)benzoxazole (DMASBO) was prepared and its absorption and fluorescence spectra were measured in various solvents. The absorption spectra are less sensitive to the solvent polarity while the fluorescence spectra are highly solvatochromic leading to a large Stokes shift. An analysis of the solvatochromic behaviour of the fluorescence spectra in terms of $\Delta f(\varepsilon,n)$ revealed that the emission occurs from a highly polar excited state. The large dipole moment change together with the strongly red-shifted fluorescence, as the solvent polarity is increased, demonstrate the formation of an intramolecular charge-transfer state (ICT). The pK_a-values of nitrogen protonation in both ground and excited states were estimated in aqueous solutions. The quantum yields of fluorescence and *trans* $\rightleftharpoons$ *cis* photoisomerization were determined in different solvents. Although a low ϕ_f-value was found in all the investigated solvents (except in viscous media) the *trans*/*cis* isomerization occurs with substantial quantum yield. The role of the ICT state in the *trans*/*cis* isomerization and fluorescence quenching was also discussed.

Keywords: Styrylbenzoxazole; Intramolecular charge-transfer; Solvent effect; Prototropic equilibrium; Photoisomerization

1. Introduction

With the advent of fluorescent whitening agents, wavelength converters and scintillators, the synthesis of highly fluorescent compounds has gained considerable interest. In benzoxazole series, in particular, 2-aryl-substituted compounds are highly fluorescent [1] exhibiting a dual fluorescence with large Stokes shift. Systems of this type have been widely used as effective light protectors as well as materials in continuous lasers [2]. Benzoxazole derivatives have also numerous therapeutic applications where some of them act as a potent antiinflammatory [3], antifungal and antibacterial agents [4]. Other applications are in electroluminescent devices [5] and UV-stabilization of polymers [6].

Aromatic compounds possessing electron donor–acceptor chromophores and exhibiting dual fluorescence are of particular interest [7] because the additional fluorescence is usually associated with the formation of a highly polar excited electronic state. Such a polar state is due to an electron transfer process and is referred as an intramolecular charge transfer (ICT) state. Charge transfer states have large dipole moments, so the energies of the excited state are expected to be highly sensitive to the solvent polarity. The charge transfer process is involved in many highly significant naturally occurring mechanisms such as vision and photosynthesis [8]. 2-Phenylbenzoxazoles carrying an amino or dimethylamino group at the *p*-position of the phenyl ring offer this advantage [9]. In these compounds the amino group acts as electron donor while the benzoxazole ring acts as the acceptor. Although the ICT process in a variety of fluorescent probes have been extensively studied by both steady state and time resolved fluorescence spectroscopy [10–12], little is known about this process in benzoxazole derivatives [9].

It seemed, therefore, of interest to study the emission characteristics, prototropic and the *trans* $\rightleftharpoons$ *cis* photoisomerization of a new fluorescent probe : 2-(*p*-dimethylaminostyryl)benzoxazole, DMASBO, to see the effect of the ICT process on the photophysical and photochemical characteristics of such a stilbene-like molecule.

2. Experimental section

2.1. Materials

Trans 2-(*p*-dimethylaminostyryl)benzoxazole (DMASBO, Scheme 1) was synthesized in our laboratory by condensa-

1010-6030/99/$ – see front matter
PII: S1010-6030(98)00439-0

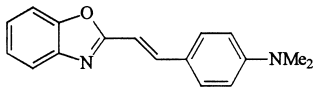

Scheme 1.

tion of 2-methylbenzoxazole with *p*-dimethylaminobenzaldehyde as reported previously [13]. The product was recrystallized twice from dry ethanol to yield yellow crystals (mp 175–177°C). DMASBO was characterized by elemental analysis; Calcd. (found) for $C_{17}H_{16}N_2O$ is: C = 77.27 (77.4), H = 6.06 (5.96), N = 10.6 (10.43)). Also, the IR spectrum (as KBr pellet) shows vibrational frequencies at 1635 and 1605 cm^{-1} characteristics for the ethylenic C=C double bond as well as at 965 cm^{-1} due to =C–H out of plane bending vibration of *trans*-olefin. The purity of the product was checked by UV–Vis and fluorescence spectral measurements.

Spectroscopic grade solvents (from Aldrich or Merck) were used as received. All the solvents were found to be non-fluorescent in the region of fluorescence measurements. Double distilled water was used for buffer solutions. Analytical grade orthophosphoric acid and NaOH were also used as received.

Absorption and fluorescence spectra were recorded on a Shimadzu UV-3101 PC spectrophotometer and a Perkin–Elmer LS 50B scanning spectrofluorimeter, respectively. Both techniques are equipped with a thermostated cell holder. Continuous irradiation was carried out by using Xe-lamp of the fluorimeter where the intensity and wavelength of the excitation light could be controlled easily. The intensity of the irradiation light was measured by application of ferrioxalate actinometry [14]. Fluorescence quantum yields were determined using solutions having absorbances around 0.1 at the excitation wavelength (usually 366 nm) and referred to 9,10-diphenylanthracene as a standard [15]. For *trans* ⇌ *cis* quantum yield determination the method described by Gauglitz [16] was used. The molar absorption coefficient of the *cis* isomer at irradiation wavelength was determined according to the modified method of Blanc and Ross [17].

Aqueous buffer solutions were made by mixing appropriate volumes of dilute (10^{-2} mol dm^{-3}) NaOH and H_3PO_4 solutions containing 50% (v/v) DMF due to the very poor solubility of DMASBO in water. Solutions of pH < 2 were made following Hammett's acidity function (H_0) scale [18]. The concentration of the solute was 2×10^{-5} M.

3. Results and discussion

3.1. Absorption and emission characteristics of DMASBO in different solvents

Table 1 summarizes the spectral properties of DMASBO in a series of solvents. In general, there is a red shift in both the absorption and emission maxima with increasing the solvent polarity. The observed bathochromic shift together with the high molar absorpitivities ($\varepsilon_{max} > 45\,000$ M^{-1} cm^{-1}) indicate that the electronic transition is analogous to the strongly allowed π–π^* transition and the lowest lying excited state is $^1(\pi\pi^*)$ [19].

Table 1
Spectral properties of DMASBO in different solvents

Solvent	λ_a (nm)	ε_{max} (M^{-1} cm^{-1})	λ_f (nm)	$\Delta\bar{\nu}$ (cm^{-1})
H_2O	387	–	525	6792
Formamide	396	57651	501	5293
Methanol	394	49409	488	4889
EtOH	394	47527	482	4634
1-Propanol	394	49384	473	4239
2-Propanol	392	48333	469	4188
1-Butanol	394	48768	468	4013
Glycerol	405	33684	497	4570
Et. glycol	402	46667	497	4817
Cyclohexanol	396	47796	466	3794
DMSO	397	43886	493	4905
DMF	394	47527	488	4889
CH_3CN	387	48602	485	5221
Acetone	388	49905	478	4852
CH_2Cl_2	390	48602	468	4273
$CHCl_3$	391	48483	463	3977
CCl_4	384	47441	451	3869
Et. acetate	385	50995	463	4376
Cyclohexane	377	49810	436	3589
n-Heptane	376	47962	435	3607
n-Hexane	375	51398	433	3572

EtOH: ethanol, Et. glycol: ethylene glycol, DMSO: dimethylsulphoxide, DMF: dimethyl formamide, Et. acetate: ethyl acetate.

The fluorescence spectra shown in Fig. 1 were normalized to highlight the differences in the peak positions. The high solvatochromaticity and broad featureless of the emission spectra indicate an intramolecular charge transfer nature of the excited state. Also, it should be noticed that the absorption maximum of DMASBO in water is blue shifted ($\lambda^a_{max} = 387$ nm) while the emission maximum is highly red shifted ($\lambda^f_{max} = 525$ nm) compared to relatively less polar protic solvents such as EtOH ($\lambda^a_{max} = 394$, $\lambda^f_{max} = 482$ nm). This can be considered as an evidence of the ICT nature of the excited state and explained on the basis of this assignment. The blue-shifted absorption maximum is due to specific hydrogen bonding interactions between water molecules and the nitrogen atom of the $-NMe_2$ group which restrict the charge transfer process. As well, the red-shifted emission maximum reveals that the transition is due to charge transfer state arising from a relatively non-polar ground state.

Fig. 1 shows also that the emission spectra of DMASBO are structured in non-polar solvents such as *n*-hexane ($\lambda_f = 415$, 433, 461 nm), and the long-wavelength shoulder extends to over 560 nm, also, a slight hint of a structured emission is apparent in CCl_4 and $CHCl_3$. The appearance of this dual fluorescence may be due to the participation of a

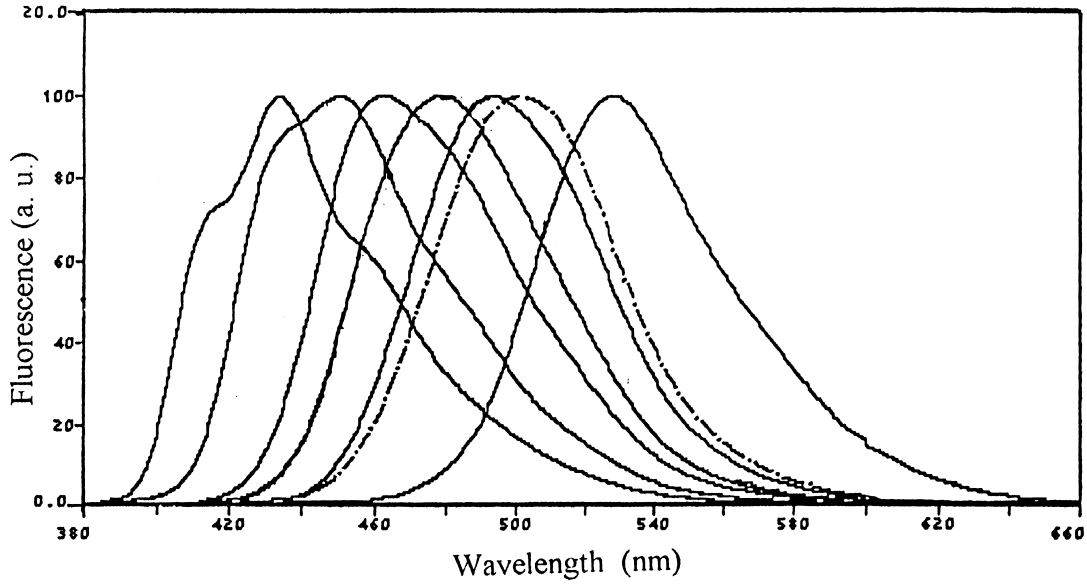

Fig. 1. Normalized fluorescence spectra of DMASBO in; *n*-hexane, CCl_4, $CHCl_3$, acetone, DMSO, formamide and water in the direction of spectral shift to longer wavelength.

second luminescent state under these lower polarity conditions. The dual fluorescence as well as the strong solvatochromaticity suggest the existence of two fluorescent states, one being the so called locally excited (LE), (primary excited Franck–Condon) state, and the second being the ICT state. It is debatable whether the ICT state is directly populated by absorption or is created by an excited state process. However, the less sensitivity of the absorption maximum to the solvent polarity, data in Table 1, supports the latter case [20,21]. Thus, it could be concluded that the ICT state is derived following relaxation of the initially formed Franck–Condon excited state. Similar photophysical mechanisms have been put forward [20] to account for the fluorescence solvatochromism of the diphenyl-hexatrienes. This conclusion is also supported by the finding that the static fluorescence spectra of DMASBO exhibit a much larger Stokes shift as the solvent polarity is increased, see Table 1. The Stokes shift increases from 3572 to 6792 cm^{-1} on changing the solvent from *n*-hexane to water, respectively, this behaviour is the well known manifestation of the charge transfer character of the solvent relaxed emissive state.

The excited state dipole moment of the fluorescent molecule can be calculated from the solvatochromic comparison methods [22]. According to these methods

$$\bar{\nu}_a - \bar{\nu}_f = F_1(\varepsilon, n)\frac{2(\mu_e - \mu_g)^2}{hca^3} + C_1 \quad (1)$$

$$\frac{1}{2}(\bar{\nu}_a + \bar{\nu}_f) = -F_2(\varepsilon, n)\frac{2(\mu_e^2 - \mu_g^2)}{hca^3} + C_2 \quad (2)$$

where

$$F_1(\varepsilon, n) = \frac{2n^2+1}{n^2+2}\left(\frac{\varepsilon - 1}{\varepsilon + 2} - \frac{n^2-1}{n^2+2}\right) \quad (3)$$

$$F_2(\varepsilon, n) = \frac{F_1}{2} + \frac{3}{2}\left[\frac{n^4-1}{(n^2+2)^2}\right] \quad (4)$$

$\bar{\nu}_a$ and $\bar{\nu}_f$ are the absorption and emission frequencies, respectively, μ_e and μ_g are the dipole moments in the excited and ground states, respectively. a is the Onsager cavity radius, ε and n are the dielectric constant and the refractive index of the solvent, respectively.

Plots of $(\bar{\nu}_a - \bar{\nu}_f)$ Stokes shift versus $F_1(\varepsilon,n)$ and $\frac{1}{2}(\bar{\nu}_a + \bar{\nu}_f)$ versus $F_2(\varepsilon,n)$ are shown in Fig. 2. The plots are clearly bilinear, within the experimental error. This suggests that the charge transfer character of the emitting state, and hence the dipole moment in the protic solvents are different from those in aprotic solvents. Omitting water, the usual regression analysis of the data yields the following equations:

(1) for protic solvents:

$$\bar{\nu}_a - \bar{\nu}_f = 7843\ F_1(\varepsilon, n) - 1803 \quad n = 9 \quad (5)$$

$$\frac{1}{2}(\bar{\nu}_a + \bar{\nu}_f) = -11009\ F_2(\varepsilon, n) + 30482 \quad n = 6 \quad (6)$$

(2) for aprotic solvents:

$$\bar{\nu}_a - \bar{\nu}_f = 1543\ F_1(\varepsilon, n) + 3590 \quad n = 12 \quad (7)$$

$$\frac{1}{2}(\bar{\nu}_a + \bar{\nu}_f) = -3990\ F_2(\varepsilon, n) + 25738 \quad n = 11 \quad (8)$$

In all cases the correlation coefficients are in the range 0.92–0.96, and were determined for the given number of solvents (n).

It could be easily observed from Fig. 2 and the slopes of correlations (5)–(7) that the Stokes shift is highly sensitive to polarity changes in protic solvents than in aprotic ones. The ratio of the dipole moment in the S_1 state (μ_e) to that in the S_0

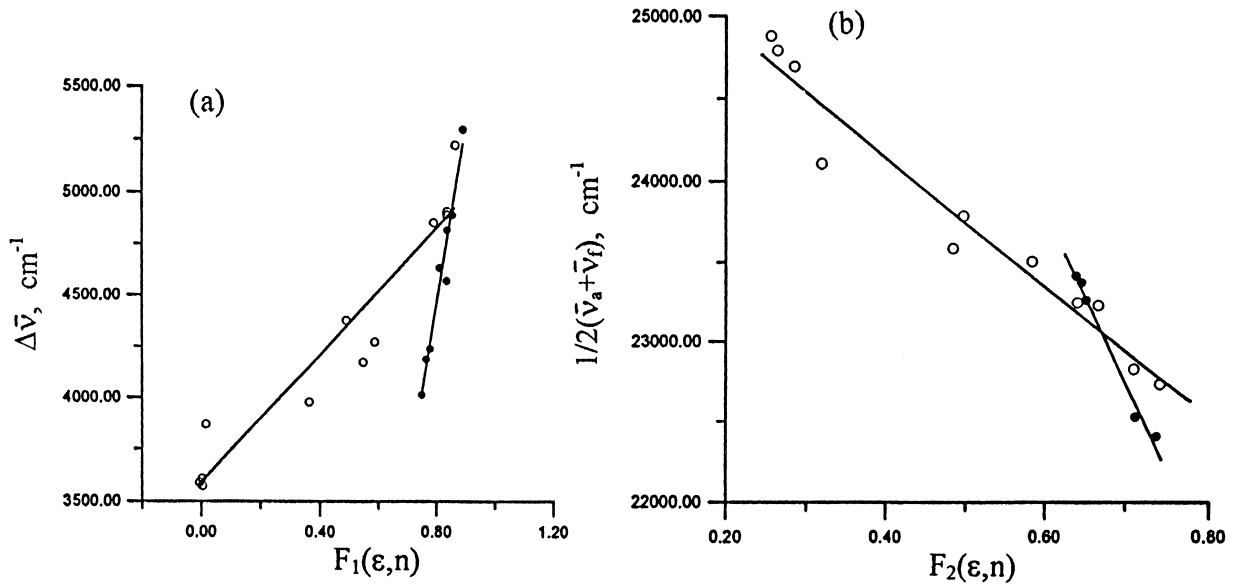

Fig. 2. Plots of: (a) stokes shift ($\Delta\bar{\nu}$) vs. $F_1(\varepsilon,n)$ and, (b) $1/2(\bar{\nu}_a + \bar{\nu}_f)$ vs. $F_2(\varepsilon,n)$. Closed and open circles indicate protic and aprotic solvents, respectively.

state (μ_g) is obtained from the slopes of the plots according to Eqs. (1) and (2). The advantage of this method is that it does not require any assumption of the cavity radius. In the present case (μ_e/μ_g) equals 5.94 and 2.26 in protic and aprotic solvents, respectively. Our results lead again to the conclusion that light excitation of DMASBO populates an ICT state with a dipole moment higher than that of the ground state.

In order to obtain an insight into the various modes of solvation (e.g. specific or non-specific) which determine the absorption and fluorescence energies E(A) and E(F), respectively, the multiple, linear regression analysis approach of Kamlet et al. [23] has been used. Correlations of E(A) and E(F) were made with Taft's π^* value, an index of the solvent polarity/polarizability, the α and β values, representing the hydrogen bond donating (HBD) and accepting (HBA) ability, respectively, of the solvent. The following regressions were obtained:

$$E(\mathrm{A}) = 75.80 - 1.78(\pm 0.33)\alpha - 2.86(\pm 0.42)\pi^* - 0.54(\pm 0.51)\beta \quad (n = 21,\ r = 0.95) \tag{9}$$

$$E(\mathrm{F}) = 65.65 - 2.11(\pm 0.45)\alpha - 7.06(\pm 0.57)\pi^* - 0.29(\pm 0.68)\beta \quad (n = 21,\ r = 0.97) \tag{10}$$

It appears that solvation is mainly determined by the dipolar interaction (π^*) and hydrogen bond donation (α) of the solvent. The ratios of the regression coefficients of α and π^*, which equal 0.622 and 0.299 for E(A) and E(F), respectively, indicate that specific interactions based on HBD play a significantly great role in the shift of the absorption maximum. This result can be explained in terms of the possibility of hydrogen bonding of the solvent hydrogen atom with the dimethylamino nitrogen atom in the ground state. However, the observed red shift of both absorption and emission maximum with increasing the solvent polarity indicates that the dispersive interactions are predominant. The contribution of both non-specific and specific interactions to the solvation process is also supported by the plot of E(A) and E(F) as a function of the Dimroth–Reichardt empirical solvent polarity parameter $E_T(30)$ [24], Fig. 3. While E(A) is almost linearly correlated with $E_T(30)$, ($r = 0.80$), the data for E(F) could be represented by two lines (correlation coefficients are greater than 0.94). A double linear correlation in the case of fluorescence indicates again that the nature of the emitting state is considerably different in the two classes of solvents.

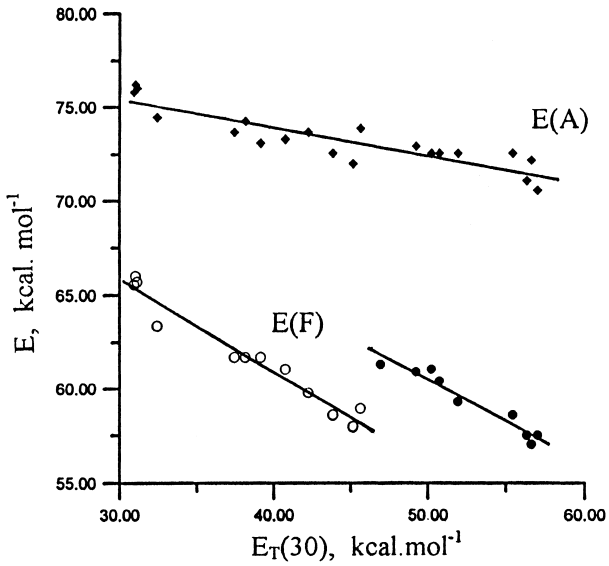

Fig. 3. Plot of E(A) and E(F) vs. the solvent polarity parameter $E_T(30)$. Symbols as in Fig. 2.

3.2. Prototropic equilibria of DMASBO

The absorption and emission spectra of the different prototropic species of DMASBO are shown in Fig. 4 while the spectral data are compiled in Table 2. As the $[H^+]$ is increased (pH < 4), in aqueous solutions containing 50% (v/v) DMF, the intensity of the absorption band at 401 nm decreases with the appearance of a new band at 326 nm. At pH = 1.5 the long-wavelength absorption band is replaced by a large red-shifted band ($\lambda_{max} = 494$ nm) and a blue-shifted band ($\lambda_{max} = 326$ nm). Also, the absorption spectra within this pH range (4–1.5) exhibit two isobestic points at 355 and 470 nm. Although DMASBO is poorly soluble in water, it is soluble enough in highly acidic aqueous solutions. At pH = 1.5, in pure aqueous solution, the long-wavelength absorption band ($\lambda_{max} = 387$ nm) is also replaced by two bands at 324 and 470 nm. However, the intensity of the band at 470 nm is very weak compared to the blue shifted one.

The fluorescence spectra, recorded at pH = 1.5, by excitation at wavelengths of the absorption band maxima are blue-shifted ($\lambda_f = 403$ nm) and red-shifted ($\lambda_f = 542$ nm), respectively, with respect to the fluorescence maximum of the neutral species ($\lambda_f = 525$ nm). These results can be explained on the basis of the ICT character of the lowest energy transition as well as the structure of DMASBO as

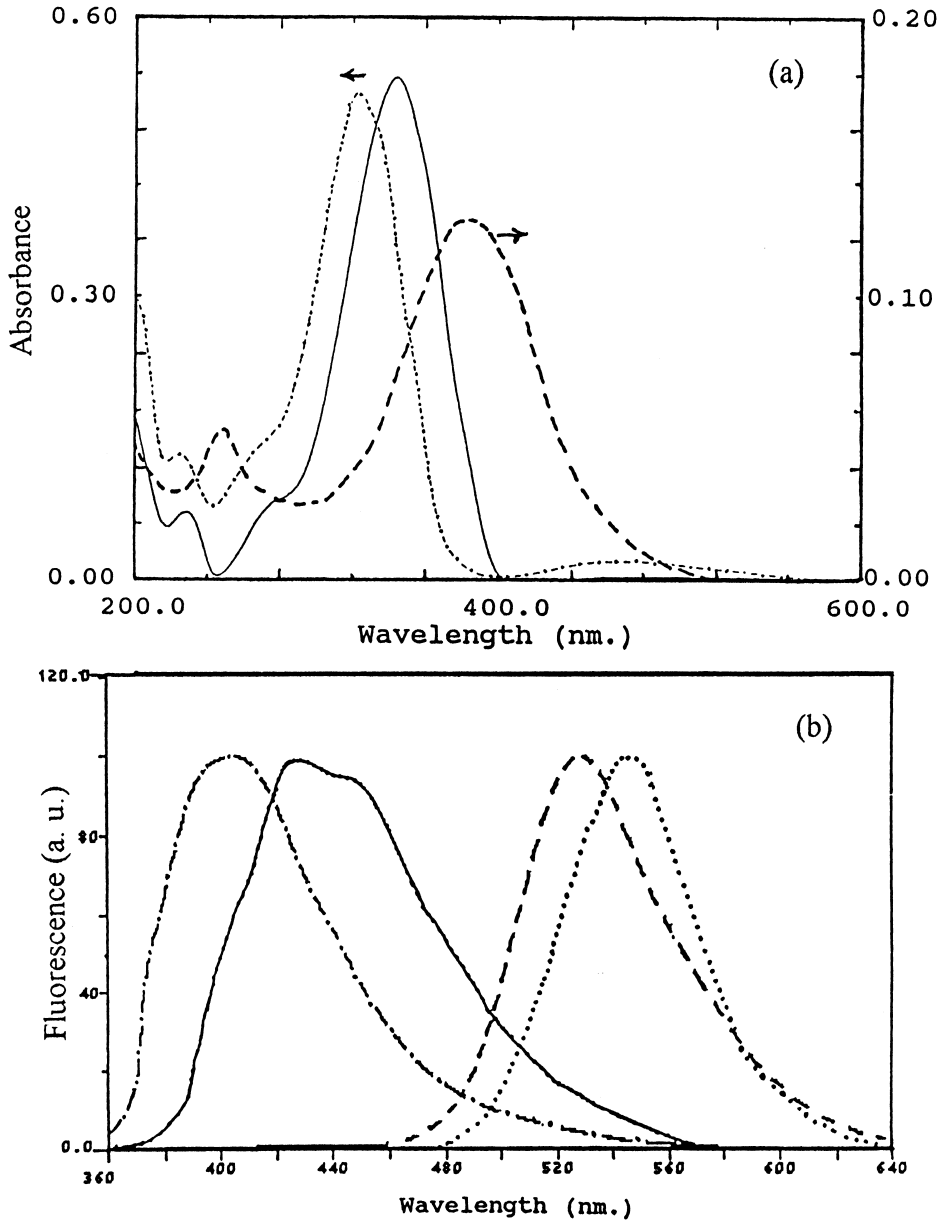

Fig. 4. (a) Absorption and (b) fluorescence spectra of the prototropic species of DMASBO; neutral (- - -), monocation I (– – –), dication (———) and monocation II (. . .) in water.

Table 2
Spectral data, ground and excited state pK_a-values of the different prototropic reactions of DMASBO

Species	λ_a (nm)		λ_f (nm)		Equilibrium	pK_a	pK_a[a]		
							FT	FC[b]	FC[c]
Neutral	387	401[a]	525	500[a]	Neutral = monocation I	2.6	2.2	−9.5	−8.0
Monocation I	324	326[a]	403	400[a]	Neutral = monocation II	2.6	–	3.9	12.2
Monocation II	470	494[a]	542		Monocation I = dication	0.1	–	3.1	3.4
Dication	343		428		Monocation II = dication	0.1	–	−10.2	−16.4

[a]Measured in 50% (v/v) DMF–water buffer solution.
[b]Calculated from the absorption maxima.
[c]Calculated from the emission maxima.
FT – fluorimetric titration; FC – forster cycle.

follows: the molecule has two protonation sites, one is the nitrogen atom of the dimethylamino group and the other is the heterocyclic nitrogen atom. So, it is expected that addition of a proton to the heterocyclic nitrogen atom will shift the absorption and fluorescence maxima to the red due to easier charge-transfer from the dimethylamino group to the benzoxazole ring. Contrary, protonation of the $-NMe_2$ group shifts the spectra to the blue in comparison to the neutral molecule. Thus, it could be concluded that the two bands in the absorption spectrum at pH = 1.5 are due to two different species which are also present in the excited state. These species, as shown in Scheme 2, are the monocations I and II.

The formation of both monocations at the same pH-value can be explained by the resonance interaction of the $-NMe_2$ group with the heterocyclic nitrogen atom, leading to structure $\bar{I}$, which stabilizes the species. The incorporation of the resonance structure $\bar{I}$ in the protolytic equilibria indicates that the proton can be added to any one of the basic centers with equal ease. Similar explanation was used to discuss the effect of acid–base concentration on the spectral properties of animo-phenylbenzothiazole and benzoxazole derivatives [9]. This is confirmed by the appearance of nice isosbestic points as well as the fact that the pK_a-values of the monocation ⇌ neutral equilibrium calculated from the spectral

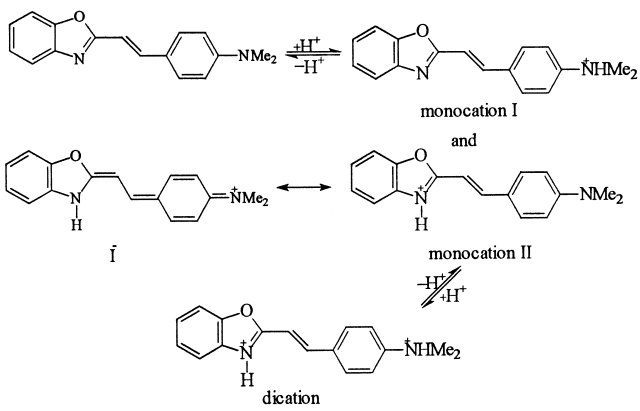

Scheme 2.

changes of the short-and long-wavelength bands are equal (pK_a = 2.6), Table 2.

Further increase of the acid concentration in completely aqueous medium, (H_o ranges from 0.9 to −4) shifts the short-wavelength absorption band (λ_a = 324 nm) to the red side (λ_a = 343 nm) while the long-wavelength band (λ_a = 470 nm) is vanished. The absorption spectra in the range pH = 1.5 to H_o = −2.66 exhibit two isosbestic points at 333 and 405 nm indicating that only two species are involved in the equilibrium. The fluorescence spectra obtained by excitation at 333 nm, for solutions having different H_o-values, suffer a red shift (λ_f = 428 nm) with a decrease in the fluorescence intensity without appearance of *iso*-emissive points. The species responsible for the red-shifted absorption and emission spectra compared to those of monocation I and blue-shifted compared to those of monocation II is assigned to the dication.

The pK_a^* values for the different prototropic reactions have been determined by Forster cycle [25] and fluorimetric titration whenever possible, Fig. 5. The pK_a^* calculated by the Forster cycle indicates that the $-NMe_2$ group becomes weaker base upon excitation, while the tertiary heterocyclic nitrogen atom becomes a stronger base. In fact, pK_a^*-values calculated using either the absorption or fluorescence spectral shifts are largely different from each other. This can be attributed to the difference in solvent relaxation of the conjugate acid–base pair in the ground and excited state. On the other hand, fluorimetric titration has resulted in the ground state pK_a-value. This indicates that the rate of the radiative decay of the conjugate acid–base pair is faster than the protonation/deprotonation rate. Consequently, the protolytic equilibrium can not be established in the excited state.

3.3. Fluorescence quantum yield and trans ⇌ cis photoisomerization

Although the emission maximum was found to be highly solvatochromic, the fluorescence quantum yield (ϕ_f), Table 3, is small and reveals virtually little dependence on the solvent polarity. Only, ϕ_f is very sensitive to changes in solvent viscosity where changing the solvent from non-

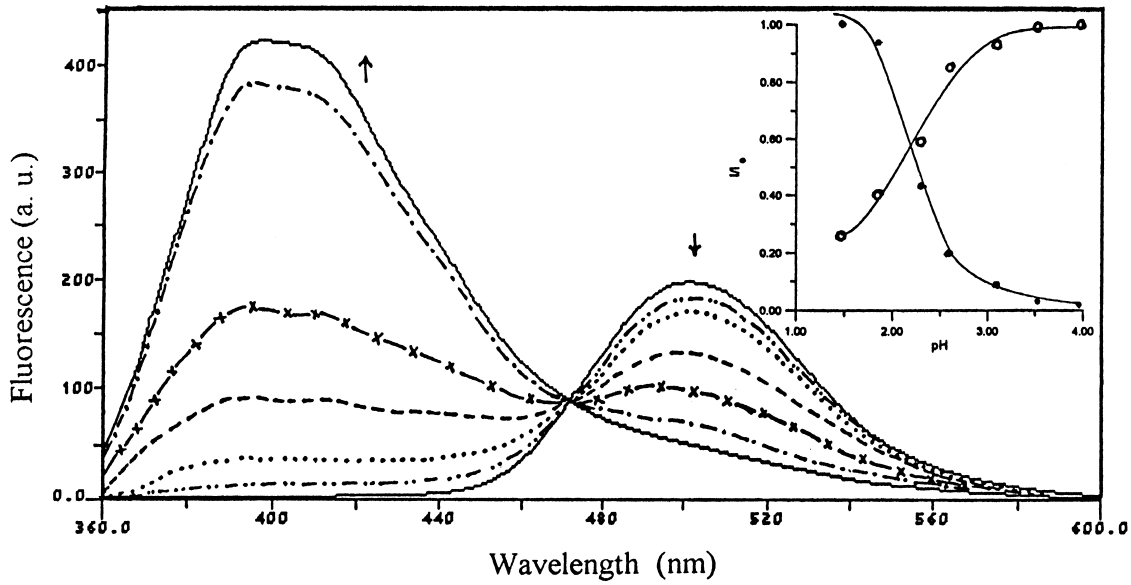

Fig. 5. Fluorescence spectra of DMASBO in 50% (v/v) DMF–water buffer solutions ($\lambda_{exc.} = 355$ nm). pH at decreasing fluorescence intensity at 400 nm is: 1.5, 1.9, 2.3, 2.6, 3.1, 3.5 and 4.0. Inset is the fluorimetric titration curves.

viscous EtOH to glycerol enhances the fluorescence quantum yield from 0.01 to 0.239. To examine further the effect of viscosity we have measured the fluorescence quantum yield of DMASBO in glycerol at different temperatures. The fluorescence quantum yield decreases on raising the temperature of the medium as shown in Fig. 6. However, the effect of changes in the refractive index of the medium at different temperatures was found to be negligible on calculating ϕ_f values [26]. Thus, the decrease in ϕ_f on heating-up of DMASBO in glycerol solutions is due to a decrease in medium viscosity. The relationship between the fluorescence quantum yield and solvent viscosity (η) is given by [27]

$$\phi_f = B(\eta/T)^x \quad (11)$$

where B and x are constants. Plot of log ϕ_f versus log (η/T) is shown in Fig. 6(b), and described by the following equation:

$$\log \phi_f = 0.594 \log(\eta/T) - 0.85 \quad (r = 0.99) \quad (12)$$

The applicability of this relation indicates that DMASBO exhibits a rotation-dependent non-radiative decay [27].

The smaller ϕ_f can result from several mechanisms. For DMASBO three possible mechanisms must be taken into consideration. One possible cause is the contribution of the n–π^* state (from the benzoxazole ring) which open the internal conversion non-radiative paths for the decay of the excited state [28]. Another possible mechanism which often produces fluorescence quenching is the ICT caused by

Table 3
Quantum yields of fluorescence (ϕ_f) and photoisomerization (ϕ_t and ϕ_c) in different solvents as well as the percentage of the *cis* isomer at the pss

Solvent	ϕ_f ($\lambda_{exc.} = 366$ nm)	$\lambda_{irr} = 366$ nm			$\lambda_{irr} = 405$ nm		
		ϕ_t	ϕ_c	*% cis*	ϕ_t	ϕ_c	*% cis*
EtOH	0.010	0.23	0.22	63	0.25	0.22	69
Methanol	0.008	0.22	0.22	63	0.22	0.22	68
DMF	0.014	0.21	0.28	55	0.23	0.30	56
CH_3CN	0.014	0.22	0.25	60	0.20	0.22	61
CH_2Cl_2	0.015	0.22	0.26	60	0.23	0.27	62
Et. glycol	0.037	0.10	0.16	49	0.11	0.19	57
Cyclohexanol	0.030	0.08	0.12	52	0.07	0.10	58
Glycerol	0.239	–	–	–	–	–	–
n-Hexane	0.015	0.21	23	62	0.22	0.25	58
H_2O	0.015	–	–	–	–	–	–
Monocation I[a]	0.049	0.15	0.17	63	0.16	0.20	75
Monocation II	<0.001	–	–	–	–	–	–

[a]Irradiation wavelengths were 313 and 334 nm instead of 366 and 405 nm, respectively.

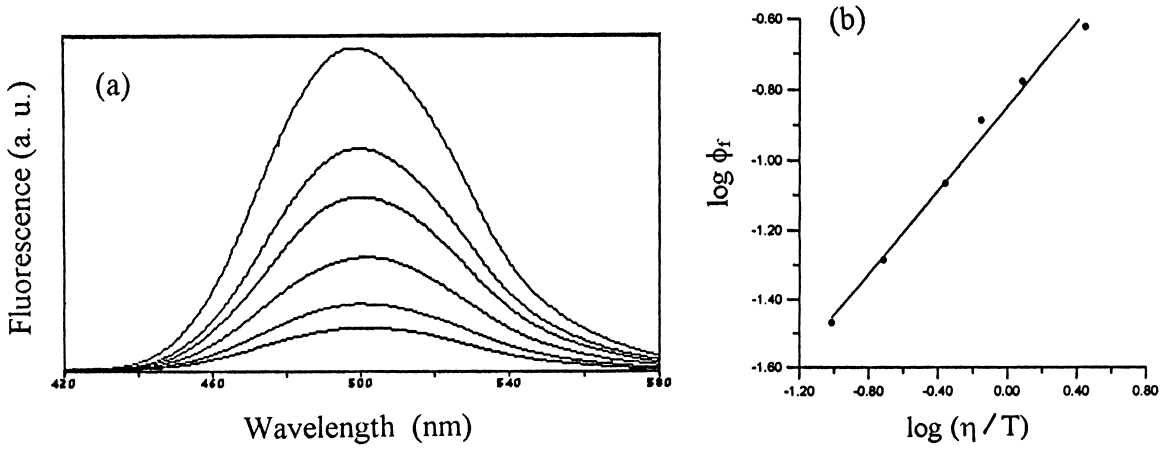

Fig. 6. (a) The changes in the fluorescence spectra ($\lambda_{exc.} = 366$ nm) of DMASBO in glycerol solution as a result of changing temperature. Temperatures at decreasing fluorescence intensity are 26, 36, 43, 52 and 64°C (b) plot of log ϕ_f vs. log η/T.

charge separation after excitation. However, in highly polar protic solvents (e.g. water) ϕ_f is higher than in less polar protic ones as EtOH. This agree extremely well with the solvent dependence of the absorption spectra and can be attributed, as shown previously, to hydrogen bonding interactions. The effect of hydrogen bonding on the fluorescence quantum yield is also demonstrated by the higher and lower ϕ_f-values of the monocations I and II, respectively. In monocation I, the protonation destroys totally the charge transfer interaction of the lone-pair electrons of the $-NMe_2$ group with the *p*-electrons of the aromatic ring, thus decreasing the non-radiative decay rates. On the other hand, in monocation II the protonation creates a positive charge on the benzoxazole ring, thus enhancing the CT interaction and increasing the rates of the radiationless processes.

In addition, the radiationless *trans*/*cis* isomerization competes successfully with the emission process. Therefore, it was interesting to determine the quantum yields of *trans* → *cis* (ϕ_t) and *cis* → *trans* (ϕ_c) photoisomerization which may provide information on the mechanism of the photoreaction and the role of charge transfer in the *cis* ⇌ *trans* isomerization process.

Upon irradiation of *trans* DMASBO in EtOH solution, as an example, at 25°C the absorbance of the band at $\lambda_{max} = 394$ nm decreases with appearance of an isosbestic point ($\lambda_{iso} = 315$ nm), finally reaching a photostationary state (pss), Fig. 7. At the same time the absorbance of the short-wavelength band ($\lambda_{max} = 250$ nm) shows a concomitant increase. Irradiation of the pss solution in the short-wavelength band (using 254 nm) results in a partial reverse of the spectral change until a new pss is obtained. In analogy to stilbenes [29] and stilbene-like molecules [28] these spectral changes indicate that the dominant photoreaction is the reversible *trans* ⇌ *cis* isomerization around the central C=C bond of DMASBO. So, the photoproduct is assigned to the *cis* isomer. From analysis of the spectra, formation of up to 69% *cis* in the pss (% *cis*) with no discernible side reactions was found.

Values for ϕ_t and ϕ_c, Table 3, are substantial and insensitive to solvent polarity as well as irradiation wavelength. Also, ϕ_t and ϕ_c-values are smaller in viscous media. This may be due to increasing of frictional forces and decreasing in the solvent-free volume required for free rotation which are responsible for *trans*/*cis* isomerization of [30].

To conclude this section, a comparison of the quantum yields of fluorescence and isomerization, reveals that the two processes are complementary. As an evidence for this conclusion is the enhancement of ϕ_f on the expense of the radiationless *trans*/*cis* isomerization as the solvent viscosity is increased from EtOH to Et. glycol. Another evidence for this fact comes from the measurement of the fluorescence and isomerization quantum yields for monocation I at pH = 1.5. The ϕ_f-value was found to be higher while ϕ_t was relatively smaller compared to those in the organic solvents used. This behaviour may also indicate the role of the ICT in the two processes.

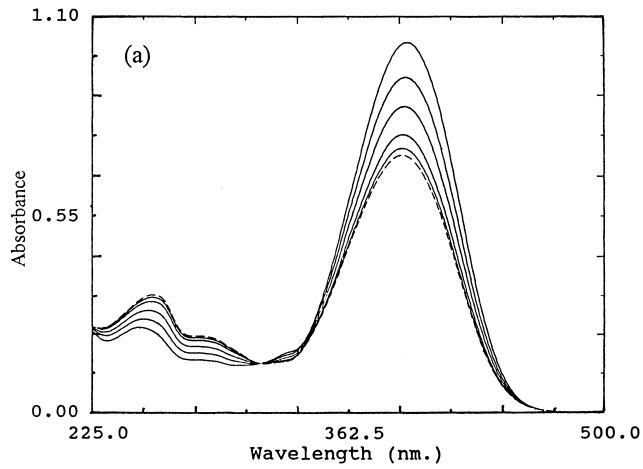

Fig. 7. (a) Effect of photo-irradiation ($\lambda_{irr.} = 405$ nm) on the absorption spectra of DMASBO in EtOH. Irradiation times at decreasing absorbances at 394 nm are 2, 5, 10, 16, 25 and 35 (pss) min.

References

[1] A. Reiser, L.J. Leyshon, D. Saunders, M.V. Mijovic, A. Bright, J. Bogie, J. Am. Chem. Soc. 94 (1972) 2414.
[2] K.P. Ghiggino, A.D. Scully, I.H. Lever, J. Phys. Chem. 90 (1986) 5089.
[3] S.F. Forgues, N. Paillous, J. Org. Chem. 51 (1986) 672.
[4] M.A. Osman, J. Am. Chem. Soc. 79 (1957) 966.
[5] N. Nakamura, S. Wakabayashi, K. Miyairi, T. Fujii, Chem. Lett. (1994) 1741.
[6] J. Irick, J.C.A. Kelly, J.C. Martin, US Patent 40 75 (1978) 126.
[7] W. Rettig, Top. Current Chem. 169 (1994) 254.
[8] H. Lueck, M.W. Windsor, W. Rettig, J. Phys. Chem. 94 (1990) 4550.
[9] J.K. Dey, S.K. Dogra, Chem. Phys. 143 (1990) 97.
[10] C.V. Kumar, L.M. Tosola, J. Photochem. Photobiol. A Chem. 78 (1994) 63.
[11] J. Catalan, C. Diaz, V. Lopez, P. Perez, R.M. Claramunt, J. Phys. Chem. 100 (1996) 18392.
[12] J. Herbich, J. Waluk, Chem. Phys. 188 (1994) 247.
[13] E.M. Vernigor, V.K. Shalaev, L.P. Novosel' tesva, E.A. Luk'yanets, A.A. Ustenko, V.P. Zvolinskii, V.F. Zakharov, Khim. Geterotsikl. Soedin 5 (1980) 604.
[14] S.L. Murov, I. Carmichael, G.L. Hug, Handbook of Photochemistry, 2nd ed., Marcel Dekker, New York, 1993.
[15] J.V. Morris, M.A. Mahaney, I.R. Huber, J. Phys. Chem. 80 (1976) 971.
[16] G. Gauglitz, J. Photochem. 5 (1976) 41.
[17] U. Steiner, M.H. Abdel-Kader, P. Fischer, H.E.A. Kramer, J. Am. Chem. Soc. 100 (1978) 3190.
[18] C.H. Rochester, Acidity Functions, Academic Press, London, New York, 1970.
[19] S. Kumar, R. Giri, J.C. Mishra, M.K. Machwe, Spectrochim. Acta 51A (1995) 1459.
[20] I.D. Johnson, E.W. Thomas, R.B. Cundall, J. Chem. Soc., Faraday Trans. 2 81 (1995) 1303.
[21] R.D. Schulte, J.F. Kauffman, Appl. Spectroscopy 49 (1995) 31.
[22] P. Suppan, J. Photochem. Photobiol. A Chem. 50 (1990) 293.
[23] M.J. Kamlet, J.M. Abboud, M.H. Abraham, R.W. Taft, J. Org. Chem. 48 (1983) 2877.
[24] C. Reichardt, Solvents and Solvent Effects in Organic Chemistry, 2nd ed., VCH, Weinheim, 1988.
[25] T. Forster, Z. Elektrochem. 54 (1950) 531.
[26] S.A. El-Daly, E.Z.M. Ebied, Spectrochim. Acta 50A (1994) 1227.
[27] R.O. Loutfy, B.A. Arnold, J. Phys. Chem. 86 (1982) 4205.
[28] U. Mazzucato, Pure Appl. Chem. 54 (1982) 1705.
[29] D.H. Waldeck, Chem. Rev. 91 (1991) 415.
[30] M.S.A. Abdel-Mottaleb, A.M.K. Sherief, L.F.M. Ismaiel, C. Deschryver, M.A. Vanderauweraer, J. Chem. Soc., Faraday Trans. 2 85 (1989) 1779.